Resistance Spot Weldability of Galvanize Coated and Uncoated TRIP Steels

Hayriye Ertek Emre * and Ramazan Kaçar

Department of Manufacturing Engineering, Karabük University, Karabük 78050, Turkey; rkacar@karabuk.edu.tr
* Correspondence: hayriyeertek@karabuk.edu.tr; Tel.: +90-370-433-8210 (ext. 1091)

Abstract: In this study, the resistance spot weldabilty of zinc galvanize-coated and uncoated TRIP800 steels was investigated in detail. Depending on the welding parameters such as welding current and welding time, the effects of zinc coating on the weld nugget geometry, the tensile shear strength, the failure modes, the hardness, and the microstructure of the resistance spot-welded sample were studied, and the results are compared with that of uncoated weldment. The coating on the surface of the TRIP steel causes a decrease in the weld nugget size and tensile shear strength of the weldment, and it changes to failure mode of the test sample from pullout to interfacial or partial interfacial fracture. As compared with the uncoated sample, the galvanized TRIP800 steel weldment has required a larger critical nugget size for achieving the desired pullout fracture mode and acceptable tensile shear strength.

Keywords: TRIP800 steel; resistance spot welding; galvanized coating; failure mode

1. Introduction

One of the most important advanced high-strength steels (AHSS's) widely used in the automotive industry is TRIP (Transformation Induced Plasticity) steel because not only is it a good candidate to facilitate gauge reduction, but it also attains an exceptional combination of strength and ductility [1,2]. TRIP steel is dominated by a ferrite matrix with retained austenite, bainite, and martensite as dispersed phases, offering excellent mechanical properties due to the transformation of retained austenite into martensite during plastic straining [3–5].

In recent years, car manufacturers have started using galvanized sheets in the automobile industry [6,7]. Two types of coatings are generally applied to steel sheets used in the automotive industry, galvanized and galvannealed coatings [8]. Pure zinc coating is called a galvanized coating, and the zinc–iron alloy is called a galvannealed coating [9]. TRIP steel sheets can be galvanized for automotive applications because of their improved corrosion resistance. Both galvanized and uncoated steels are joined in automotive applications predominantly using the resistance spot welding (RSW) process [8]. In resistance spot welding, the metal surfaces are joined by the heat obtained from the resistance to the electric current. The metal parts around the interface are heated due to this heat generation, resulting in melting and the formation of a weld pool. The weld pool solidifies and a joint (weld nugget) is produced [10]. The welding current, the welding time, and the electrode force are the most important parameters in spot welding [8]. The objective of the RSW process is to generate heat rapidly in the joints of the material being welded while minimizing the conduction of heat to the cooler adjacent material [11]. This heat generation ($Q = I^2Rt$) can be expressed, where Q is the heat energy in joules, I is the current in amperes, R is the resistance in ohms, and t is the time in seconds [12]. According to this equation, in the course of RSW, the heat input is mainly controlled by the current, time, and electrical resistance of the steel sheets. Compared to the welding of uncoated sheets, the welding of galvanized sheets requires more accurate control of welding parameters, and the weldability

range must be narrower than in the case of uncoated sheets. Weldability decreases as the thickness of the coating increases [13]. Upon heating, the coating of the sample will melt first [14,15], and the molten coating at each of the interfaces serves the contact resistances, as schematically shown in Figure 1, as compared to the uncoated steels, which were welded at the same welding parameters [15,16]. The molten zinc at the faying interface is pushed to the periphery of the contact area where it forms an annulus that contributes to shunt the welding current to further reduce the resistance of the circuit [15,17].
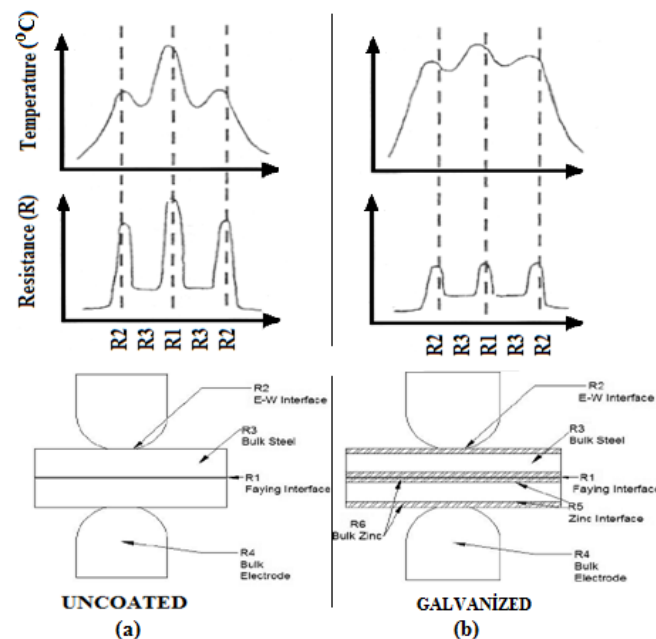

Figure 1. The resistance and resultant temperature profile for (**a**) uncoated; (**b**) galvanize-coated samples [15,16].

Generally, steel sheets were coated before RSW in the automotive industry. The optimum welding parameters can be changed by the coating the metal sheets. Thus, the automakers have to decide the optimum welding parameters for uncoated and coated steel sheets. Since it has been reported [13–17] that the zinc-galvanized coating affects the weldability of the steels negatively, it is important to determine the effect of the process parameters on the weld quality of coated and uncoated steels weldments. The extensive literature survey revealed that there has been limited research on the resistance spot weldability of uncoated and galvanize-coated TRIP steel sheets. Therefore, the effect of zinc coating on resistance spot weldability of TRIP800 steels was investigated in this study. For this purpose, the effects of welding parameters (welding current and welding time) on the nugget diameter, d_n, and the nugget height, h_n, of a weldment were investigated. Additionally, the tensile shear strength and failure mode associated with the weld nugget geometry of the spot-welded galvanized and uncoated TRIP800 steel sheets were examined under lap shear loading conditions. Failure modes were determined by observing the weld fracture surfaces. The hardness test was used to assess the weldability of the steels.

2. Materials and Methods

Galvanize coated and uncoated TRIP800 steel sheets 1.5 mm in thickness were used for the experimental study. The chemical composition of the steel is given in Table 1. The coated samples were cleaned from galvanization under laboratory conditions with an emery cloth and by rinsing in ethyl alcohol.

Table 1. The chemical composition of the TRIP800 steel (% weight).

Base Metal	C	Si	Mn	P	S	Cr	Mo	Al	Fe
TRIP800	0.2	1.66	1.69	0.015	0.0002	0.006	0.011	0.43	Balance

A timer, current-controlled AC resistance spot welding machine with a power capacity of 60 kVA, and various pneumatic application mechanisms with a single lever were used for the experiments. The weld lobe diagram is one of the most powerful techniques that can be used to illustrate determining optimum welding parameters [18,19]. A weld lobe diagram divides the welding current and the welding time domain, using two lines for the maximum and minimum currents, into three regions in terms of weld quality: undersized weldment, acceptable weldment, and expulsion [20]. Thus, the welding parameters selected associate with the weld lobe diagram, which was developed for uncoated TRIP800 samples in a previous study [18].

The welding parameters are shown in Table 2.

Table 2. Welding parameters.

Welding Current (kA)	Electrode Force (kN)	Weld Time (Cycle)	Hold Time (Cycle)	Squeeze Time (Cycle)	Clamping Time (Cycle)	Electrode Type(F16)	Electrode Diameter (mm)
6 7 8 9	6	15 20 25	15	25	15	Spherical tip (Cu–Cr–Zr)	5.5

Note: 1 cycle = 0.02 s.

All series of welded joints were exposed to a tensile shear test in order to determine joint strength. The information about the tensile shear test sample is given in Figure 2a. Five tensile shear test samples were prepared and tested for each of the weld variables by using a Shimadzu testing machine. The Vickers microhardness (Shimadzu Sanjo Works, Kyoto, Japan) measurement across the weld nugget, the heat affected zone (HAZ), and the base metal was carried out with a load of 500 g. The transverse sections of the weldment passing through the weld nugget, as well as a similar section of the base plates, were prepared by a standard metallographic procedure. An optical examination of specimens was carried out using a Nikon DIC microscope (Nikon Instruments, Karfo-Karacasulu Dis. Tic. A.S., Istanbul, Turkey) Zeiss Ultra Plus type SEM microscope (Leibniz Institute for Solid State and Materials Research, Helmholtzstraße, Dresden, Germany). Nugget diameters (d_n), the heights of the nugget (h_n) and the HAZ width were measured from the metallographic samples by an Optic and Stereo Microscope (Nikon Instruments, Karfo-Karacasulu Dis. Tic. A.S., Istanbul, Turkey), as seen in Figure 2b.
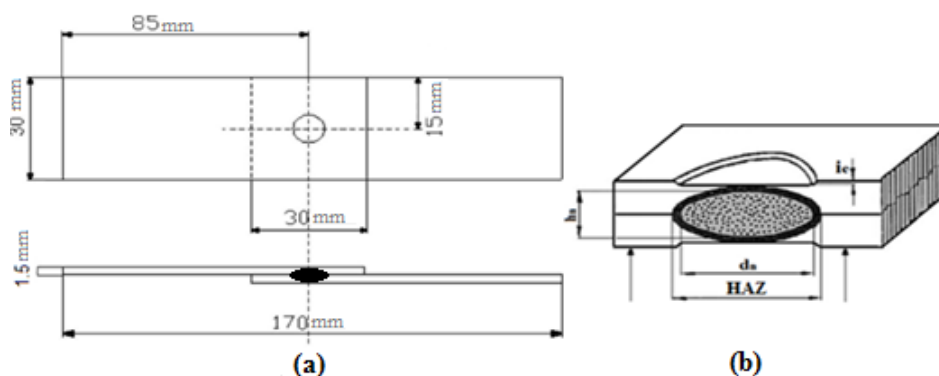
Figure 2. (**a**) The tensile shear test sample; (**b**) the transverse sections of weldment.

3. Results and Discussion

3.1. Microstructure and Nugget Geometry of the Weldment

Figure 3 illustrates the macro and the microstructure of galvanized and uncoated welded samples, which were joined with the same welding parameters. The weldment consists of three distinct structural zones: (i) the weld nugget; (ii) the heat affected zone (HAZ); and (iii) the base metal.
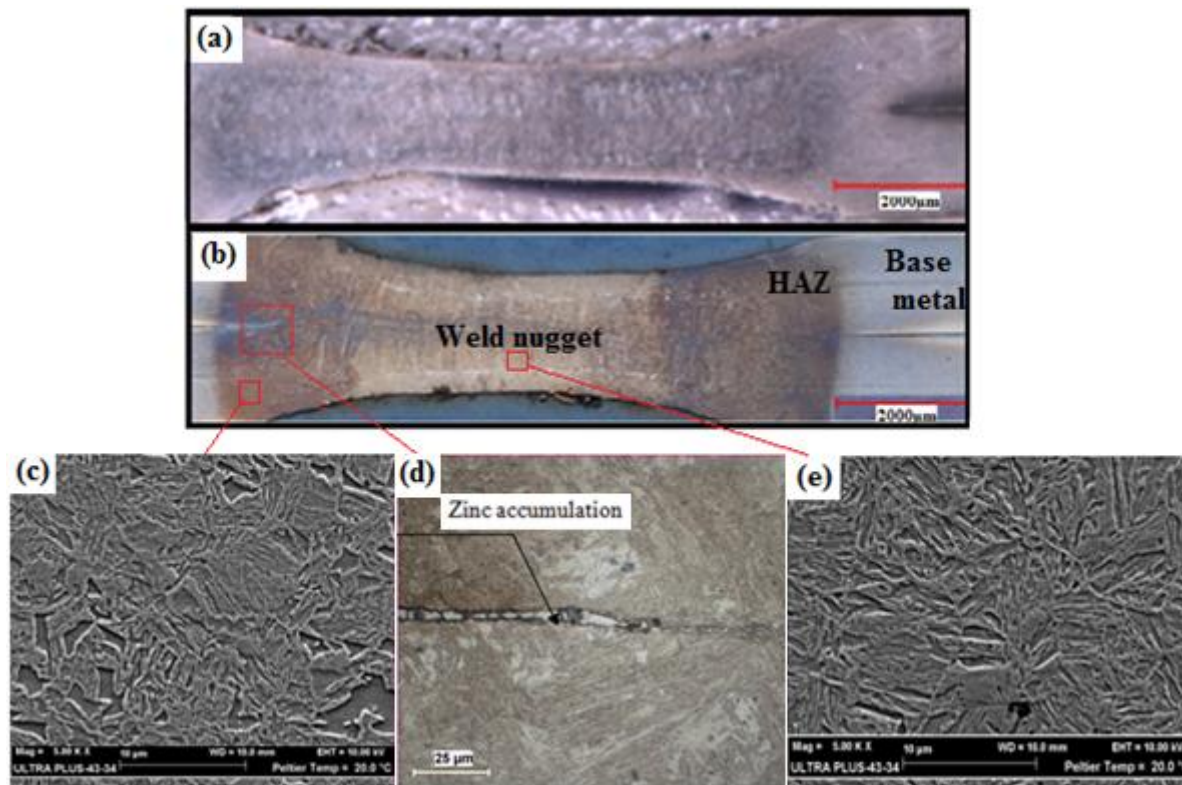

Figure 3. Macro and microstructure of spot-welded samples: (**a**) uncoated; (**b**) galvanized; (**c**) HAZ; (**d**) periphery of contact zone; (**e**) weld nugget.

As seen in Figure 3a,b, the weld nugget microstructure of the both galvanized and uncoated samples is covered by martensite phases predominantly (Figure 3e), while the martensite, bainite, and retained austenite phases present in the HAZ (Figure 3c). In Figure 3b, at the early stage of the welding, the expulsed molten zinc is evaluated on the periphery of the contact zone [21]. Li et al. [22] investigated the behavior of the zinc liquid during the welding. The authors noticed that the molten zinc is expulsed towards the periphery of the contact area to form a zinc annulus that extends to the electro-thermal contact surface during the welding stage, thereby reducing the current density crossing the interfaces.

The effects of the coating and welding parameters, such as the welding current and the welding time, on the nugget diameter and the nugget height were determined, and the findings are given graphically in Figure 4. It was confirmed that the nugget diameters of both weldments extend by increasing the heat input associate with the welding current and the welding time. Meanwhile, the nugget cross-section height decreases in high welding parameters. This might be due to the forging of the soft zone. In low welding currents achieved by increasing the welding time, the amount of fused metal to form a nucleus increase, so the nucleus diameter increases and the height of the nucleus nearly reaches the sheet thickness [23]. Using a welding current greater than 6 kA causes deeper electrode indentation; thus, the weld nugget height decreases. As seen in Figure 4, a larger nugget diameter and a thicker nugget cross-section height was determined for uncoated specimens, as compared with

galvanize-coated samples. Similar results have also been reported by other researchers [7,22–25]. Since the resistance at the sheet interfaces has shifted due to the presence of zinc, the thermal gradient across the weld parallel to the electrode axis to the electrode may still be rather small [24,25]. Raoelison et al. [21] reported that, in the case of the uncoated sample, 100% of the current crosses the sheet-to-sheet contact inside a radius of 3 mm; however, only 80% of the weld current passes through the zinc-coated weldment. According to the Joule rule, for the heat input occurring between electrodes at an electric resistance Q (calorie) $= I^2Rt$, the generated heat appears as a function of the current intensity (I), the resistance of the materials (R), and the time (t). It is believed that a higher heat input is generated for uncoated samples than for galvanize-coated samples, which results in a larger melting area and thus an extension in nugget diameter. In the case of zinc-galvanized steel sheets, however, higher welding currents are required to form a nugget with a suitable size [22,25].
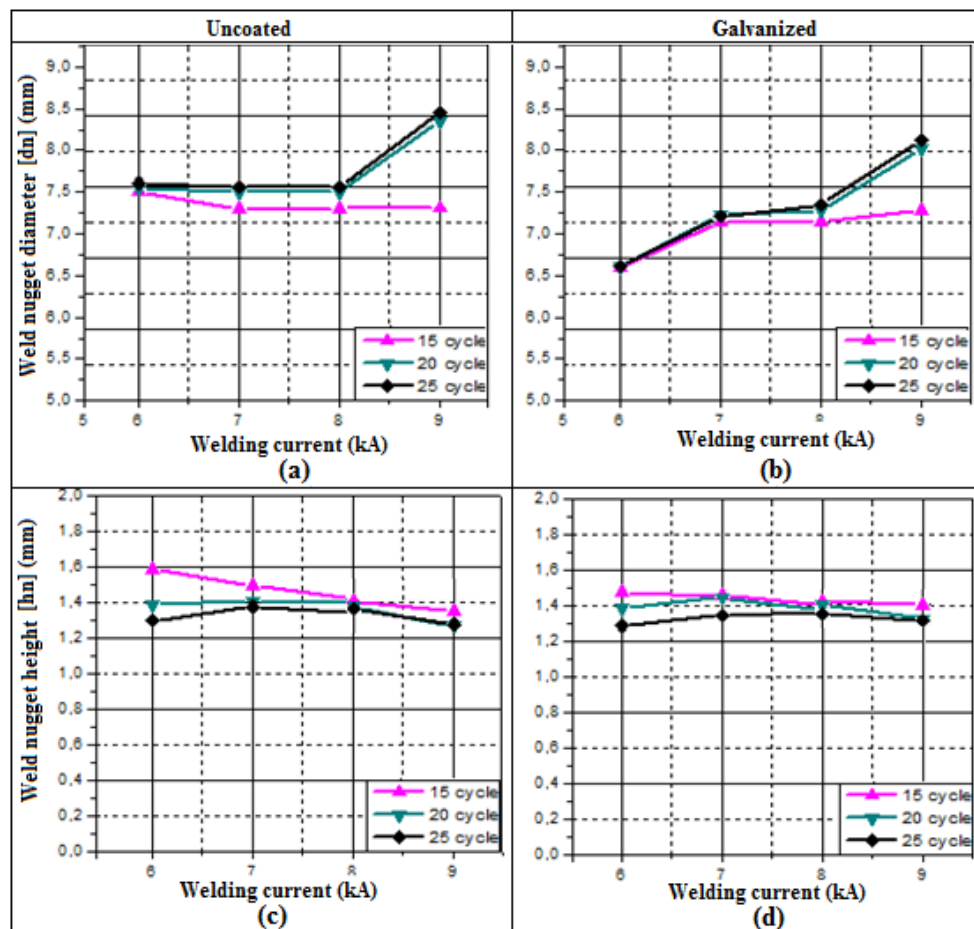

Figure 4. Effect of welding parameters on the weld nugget diameter and the nugget height of welded samples: (**a**,**c**) uncoated; (**b**,**d**) galvanized.

Figure 5 indicates that the HAZ width of both weldments enlarge with increasing welding parameters. It is worth noting that the zinc-galvanized welded sample has a larger HAZ. This could be explained by the higher thermal conductivity of the galvanized steel and an enlargement of the electro-thermal contact radius, due to the zinc accumulation or uncertainties of the experiments and the measurements (including the identification of the HAZ). Researchers [22] have also reported an enlargement of the electro-thermal contact radius due to zinc accumulation. Therefore, during resistance spot welding, an enlargement area of the contact surface to steel sheets causes a wider heating zone, which indicates an extension in the HAZ for galvanized joints.
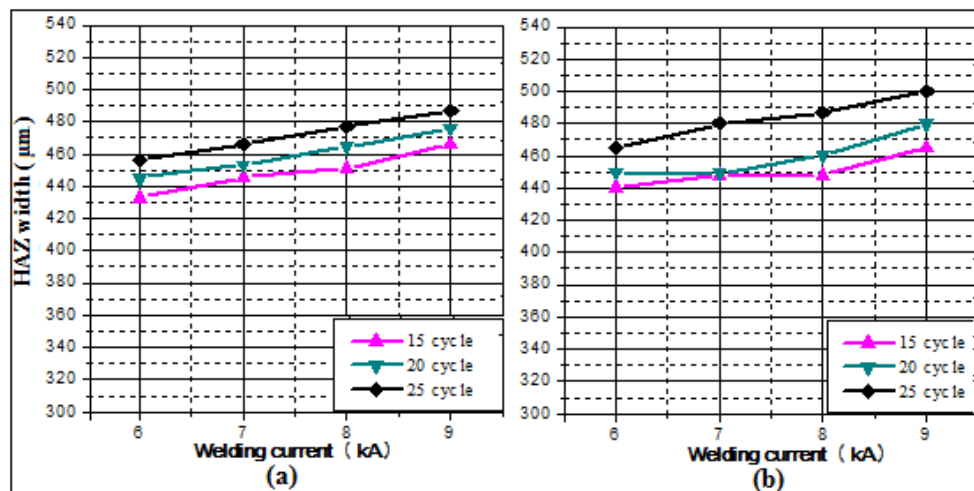
Figure 5. Effect of welding parameters on the width of the HAZ: (**a**) uncoated; (**b**) galvanized.

3.2. Tensile Shear Performance of Weldment

The effects of the welding parameters such as welding current and welding time on the tensile shear strength and failure types of both weldments were investigated, and the results are shown graphically in Figure 6a,b.
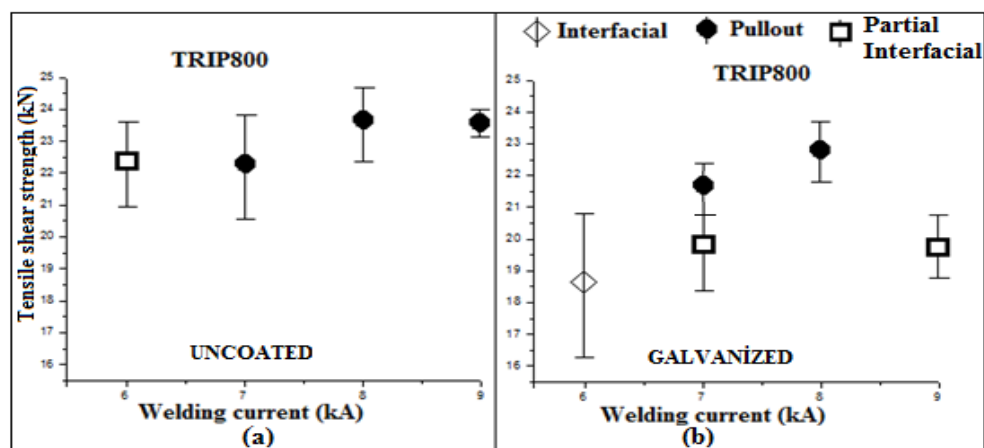

Figure 6. Effect of welding parameters on the tensile shear strength and failure types: (**a**) uncoated; (**b**) galvanized.

As seen in Figure 6a,b, the tensile shear strength of all weldments improves by increasing the heat input associated with the welding current and the welding time, except 9 kA in Figure 6b. The maximum tensile shear strength for uncoated and galvanized samples was determined to be 24.75 kN and 23.5 kN, respectively. The strength of the uncoated sample was found to be about 1.25 kN higher. The zinc-galvanized coating causes a negative effect on the strength.

The failure mode of the test samples was examined. As seen in Figure 6, an interfacial failure (IF) mode was evaluated for galvanized samples that were joined at a 6 kA welding current for all welding times. The interfacial fracture (IF) mode can be avoided by either reducing the fusion zone hardness or alternatively extending the nugget diameter for a given sheet thickness [26,27]. Increasing the heat input enabled a joining at a larger area, which resulted in a desired pullout failure (PF) mode for both weldments. A partial interfacial failure (PIF) mode was observed in the uncoated sample joined at 6 kA for all welding times due to insufficient heat input. Meanwhile, a PIF mode due to

excessive heat input was also observed in the galvanized sample joined at 9 kA for all welding times. These failure types indicate that the heat input related with the welding parameters passes through to a critical level that causes expulsion and results in a PIF type.

Studies have shown that zinc forms at the faying surface around the fusion zone during the spot welding of Zn-galvanized steel (Figure 7). Results indicate that the coating strongly affects the failure mode of the spot weldment of TRIP steels.
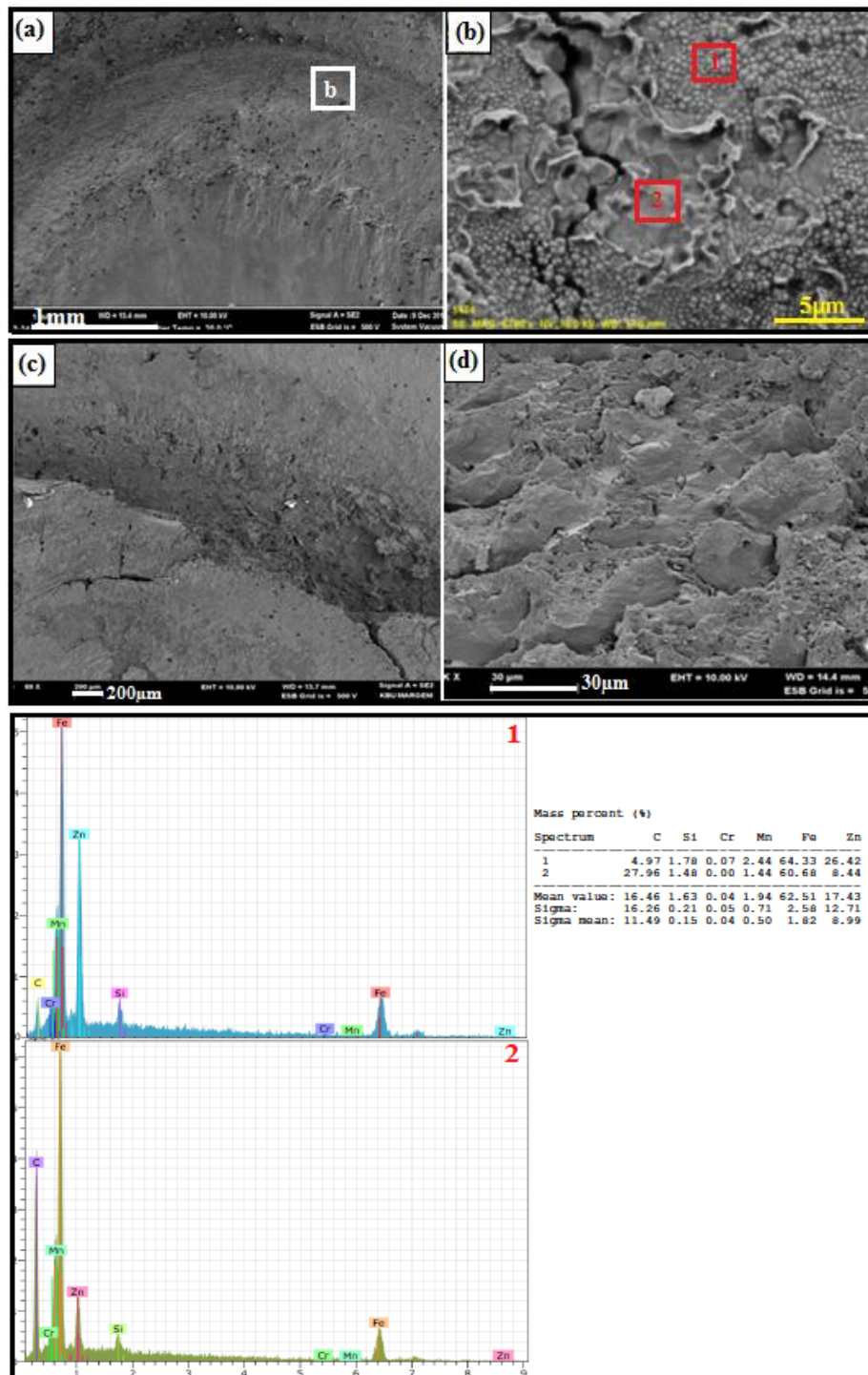

Figure 7. Failure modes: (**a**) IF mode. (**b**) Magnification view of IF mode (1 and 2 are point of EDS analysis). (**c**) PIF mode. (**d**) Magnification of PIF mode.

Figure 7 shows fracture surface of samples that were failed IF and PIF mode. They present partly brittle fracture behavior due to a hard martensite structure or a zinc-enriched region. EDS analysis was carried out on the fracture surface of the samples. Results indicate the zinc-enriched region (Figure 7b). The nature of the spot welding and the subsequent rapid cooling resulted in a martensite structure in the fusion zone due to a high amount of carbon and alloying elements. The presence of the hard martensite phase essentially allows for an easier propagation of cracks and generates interface failures more easily [27,28].

3.3. Hardness Measurement

Figure 8a,b shows the hardness profiles of spot-welded galvanized and uncoated TRIP800 steels. The hardnesses of both galvanized and uncoated base and weld metals were determined for similar welding conditions. The hardness of the base metal was found to be 250 $HV_{0.5}$, and it increased up to 550–600 $HV_{0.5}$ in the weld nugget due to martensitic transformation. The hardness in the weld nugget and the HAZ was slightly affected due to increasing welding parameters (Figure 8). This result may be explained by structural transformation during the cooling of the weldment. The HAZ hardness in the galvanized weldment was measured to be 25 $HV_{0.5}$, which is higher than that of the uncoated samples. This can be attributed to grain refinement and the increasing martensite volume fraction in the HAZ. Since the galvanized coating has a faster heat transfer, the martensite volume fraction increased.
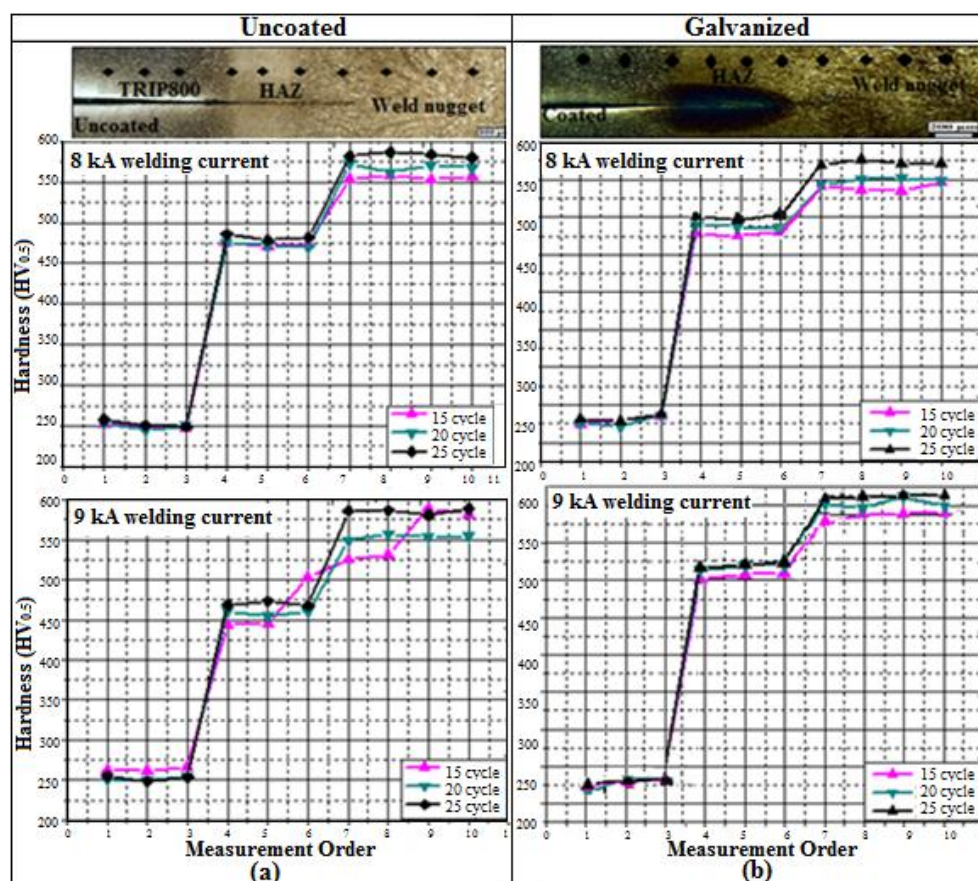

Figure 8. Hardness measurement of samples: (**a**) uncoated; (**b**) galvanized.

4. Conclusions

In this study, the effect of the welding parameters such as welding time and welding current on the weld nugget geometry, the tensile shear strength, and the hardness of the resistance of spot-weldments were investigated. From the results given above, the following conclusions can be drawn:

- The microstructure of both weldments was decorated by the predominantly martensite phases in the weld nugget. Martensite, bainite, and retained austenitic phases were evaluated in the HAZ.
- It was found that the nugget diameter increased with increasing welding currents greater than 6 kA for all welding times (15, 20 and 25 cycles). Using a welding current greater than 6 kA causes more forging of soft zones and decreases the nugget height. The galvanized coating on the surface of the TRIP steel resulted in a smaller nugget diameter and a thicker nugget cross section.
- The HAZ of the galvanized TRIP800 weldment was found to be slightly larger due to the higher thermal conductivity of the galvanized steel.
- The tensile shear strength of both weldments improves by increasing the heat input associated with the welding current and the welding time, except 9 kA. The coating presents a negative effect on the strength and failure mode.
- A partial interfacial failure (PIF) mode was observed in the uncoated sample joined at 6 kA for all welding times due to insufficient heat input. Meanwhile, a PIF mode due to excessive heat input was also observed in the galvanized sample joined at 9 kA for all welding times.
- The welding current and welding time range, to obtain indented weld nugget geometry and a desired PF mode for the uncoated sample, should be higher. Increasing the heat input up to expulsion enables joining at a larger area, which provides an extended nugget size and a desired PF mode for both weldments.
- It was found that hardness increased in the fusion zone and the HAZ of both weldments due to martensitic transformation. In addition, the HAZ hardness of the galvanized weldment was found to be slightly higher. It is believed that coating leads to the conduction of heat faster, thus preventing the coarsening of the grains in the HAZ, so fine grains cause high hardness.

References

1. Baltazar Hernandez, V.H.H.; Okita, Y.; Zhou, Y. Second pulse current in resistance spot welded TRIP steel—Effects on the microstructure and mechanical behavior. *Weld. J.* **2012**, *91*, 278–285.
2. Keeler, S.; Kimchi, M. Advanced High Strength Steel (AHSS). *Application Guidelines, Committee on Automotive Applications*, Version 5.0. Word Auto Steel, Ed.; 2014; 1–4.
3. Word Auto Steel. Available online: http://www.worldautosteel.org/Projects/AHSS-Guidelines.aspx (accessed on 13 April 2010).
4. Lacroix, G.; Pardoen, T.; Jacques, P.J. The fracture toughness of TRIP-assisted multiphase steels. *Acta Mater.* **2008**, *56*, 3900–3913. [CrossRef]
5. Brauser, S.; Pepke, L.A.; Weber, G.; Rethmeier, M. Deformation behaviour of spot-welded high strength steels for automotive applications. *Mater. Sci. Eng. A* **2010**, *527*, 7099–7108. [CrossRef]
6. Bian, J.; Zhu, Y.; Liu, X.H.; Wang, G.D. Development of hot dip galvanized steel strip and its application in automobile industry. *J. Iron Steel Res. Int.* **2006**, *13*, 47–50. [CrossRef]
7. Hayat, F. Comparing properties of adhesive bonding, resistance spot welding, and adhesive weld bonding of galvanized and uncoated DP 600 steel. *J. Iron Steel Res. Int.* **2011**, *18*, 70–78. [CrossRef]
8. Tumuluru, M. Effect of coatings on the resistance spot welding behavior of 780 MPa dual-phase steel. *Weld. J.* **2007**, *86*, 161–169.
9. Tumuluru, M. Effects of baking on the structure and properties of resistance spot welds in 780 MPa dual-phase and TRIP steels. *Weld. J.* **2010**, *89*, 91–100.
10. Amırthalingam, M.; Master of Science in Metallurgical and Materials Engineering. *Microstructural Development during Welding of TRIP Steels*; Indian Institute of Technology: Madras, Chennai, India, 2010.
11. Arunchai, T.; Sonthipermpoon, K.; Apichayakul, P.; Tamee, K. Resistance spot welding optimization based on artificial neural network. *Int. J. Manuf. Eng.* **2014**, *2014*, 154784. [CrossRef]

12. Williams, N.T.; Parker, J.D. Review of resistance spot welding of steel sheets-Part 2 Factors influencing electrode life. *Int. Mater. Rev.* **2014**, *49*, 77–108. [CrossRef]

13. Ruuki Part of SSAB. Available online: http://www.ruukki.com/~/media/Files/Steel-products/Cold-rolled-metal-colour-galvanized-instructions/Ruukki-Resistance-welding-manual.pdf (accessed on 3 August 2014).

14. Roach, B.W. Welding modern coated materials. *Weld. Met. Fabr.* **1988**, *56*, 167–170.

15. Chan, K.R. Weldability and Degradation Study of Coated Electrodes for Resistance Spot Welding. Master's Thesis, University of Waterloo, Waterloo, ON, Canada, 2005.

16. Finlay, M.R. A study of resistance spot weldability of metallic coated steels and PVD coated electrodes. Master's Thesis, University of Wollongong, Wollongong, New South Wales, Australia, 1995.

17. Howe, P.; Kelly, S.C. A comparison of the resistance spot weldability of bare, hot-dipped, galvannealed, and electrogalvanized DQSK sheet steels. In Proceedings of the International Congress and Exposition, Detroit, MI, USA, 29 February–4 March 1988.

18. Emre, H.E.; Kaçar, R. Development of weld lobe for resistance spot-welded TRIP800 steel and evaluation of fracture mode of its weldment. *Int. J. Adv. Manuf. Technol.* **2016**, *83*, 1737–1747. [CrossRef]

19. Cho, Y.; Li, W.; Hu, S.J. Design of experiment analysis and weld lobe estimation for aluminum Resistance spot welding. *Weld. J.* **2006**, *85*, 45–51.

20. Zhang, H.; Senkara, J. *Resistance Welding: Fundamentals and Applications*, 2nd ed.; CRC Press: New York, NY, USA, 2012; p. 197.

21. Raoelison, R.; Fuentes, A.; Rogeon, P.H.; Carré, P.; Loulou, T.; Carron, D.; Dechalotte, F. Contact conditions on nugget development during resistance spot welding of Zn galvanized steel sheets using rounded tip electrodes. *J. Mater. Process. Technol.* **2012**, *212*, 1663–1669. [CrossRef]

22. Li, M.V.; Dong, P.; Kimchi, M. Finite element modeling of resistance spot welding of galvanized steel. In Proceedings of the International Conference on Computer Technology in Welding, San Francisco, CA, USA, 8–11 July 1997; pp. 389–398.

23. Aslanlar, S. The effect of nucleus size on mechanical properties in electrical resistance spot welding of sheets used in automotive industry. *Mater. Des.* **2006**, *27*, 125–131. [CrossRef]

24. Chan, K.R.; Scotchmer, N.; Zhao, J.; Zhou, Y. Weldability Improvement Using Galvanized Electrodes for RSW of HDG Steel, SAE International Huys Industries Limited, 2005. Available online: http://huysindustries.com/data/uploads/articles/huysarticle04.pdf (accessed on 3 August 2014).

25. Rogeon, P.H.; Carré, P.; Costa, J.; Sibilia, G.; Saindrenan, G. Characterization of electrical contact conditions in spot welding assemblies. *J. Mater. Process. Technol.* **2008**, *195*, 117–124. [CrossRef]

26. Howe, P.; Kelly, S.C. Coating weight effect on the resistance spot weldability of electrogalvanized sheet steels. *Weld. J.* **1988**, *67*, 271–280.

27. Shi, G.; Westgate, S.A. Techniques for improving the weldability of TRIP steel using resistance spot welding. *Int. J. Join. Mater.* **2004**, *16*, 9–14.

28. Ma, C.; Chen, D.L.; Bhole, S.D.; Boudreae, G.; Lee, A.; Biro, E. Microstructure and fracture characteristics of spot-welded DP600 steel. *Mater. Sci. Eng. A* **2008**, *485*, 334–346. [CrossRef]